Nanoscale

PAPER

View Article Online
View Journal | View Issue

Cite this: *Nanoscale*, 2017, **9**, 9026

An efficient enzyme-powered micromotor device fabricated by cyclic alternate hybridization assembly for DNA detection†

Shizhe Fu, Xueqing Zhang, Yuzhe Xie, Jie Wu * and Huangxian Ju

An efficient enzyme-powered micromotor device was fabricated by assembling multiple layers of catalase on the inner surface of a poly(3,4-ethylenedioxythiophene and sodium 4-styrenesulfonate)/Au microtube (PEDOT-PSS/Au). The catalase assembly was achieved by programmed DNA hybridization, which was performed by immobilizing a designed sandwich DNA structure as the sensing unit on the PEDOT-PSS/Au, and then alternately hybridizing with two assisting DNA to bind the enzyme for efficient motor motion. The micromotor device showed unique features of good reproducibility, stability and motion performance. Under optimal conditions, it showed a speed of 420 μm s^{-1} in 2% H_2O_2 and even 51 μm s^{-1} in 0.25% H_2O_2. In the presence of target DNA, the sensing unit hybridized with target DNA to release the multi-layer DNA as well as the multi-catalase, resulting in a decrease of the motion speed. By using the speed as a signal, the micromotor device could detect DNA from 10 nM to 1 μM. The proposed micromotor device along with the cyclic alternate DNA hybridization assembly technique provided a new path to fabricate efficient and versatile micromotors, which would be an exceptional tool for rapid and simple detection of biomolecules.

Received 16th February 2017,
Accepted 28th May 2017

DOI: 10.1039/c7nr01168g

rsc.li/nanoscale

Introduction

Chemically powered micro/nanomotors inspired by the biomachines of nature are artificial devices.[1–5] They achieve autonomous movement by converting chemical energy into kinetic energy.[6] Since the pioneering reports on nanoswimmers,[7,8] the rapid development of chemically powered micro/nanomotors has been witnessed. The research studies of artificial micro/nanomotors mainly focus on two aspects: the exploration of the motion mechanism[9–12] and their applications in various areas including drug delivery,[13–17] isolation of biological targets,[18–20] environmental monitoring,[21–26] and energy supply.[27]

Due to the advantages of simple preparation, mass production, low cost, shape and composition diversity, and autonomous movement, artificial micro/nanomotors have been widely used in biosensing. Based on the specific silver-related speed of catalytic nanowire motors,[28] Wang's group pioneered the application of artificial nanomotors in DNA detection.[29] However, the further application of nanowire motors in complex media has been limited due to their inactivation in a high ionic-strength media environment.[30] Tubular micromotors with bubble-induced propulsion have been proposed to overcome this limitation, thus greatly promoting the development of motor-based biosensing platforms.[31,32]

Normally, tubular micromotors show a double cone shape, in which the inner layer acts as the engine to produce propulsion and the outer layer is used to immobilize various biorecepetors[33] and construct the sensing interface for the detection of proteins,[34] DNA,[35] nerve agents,[36] and cells.[18] These tubular micromotors can perform "on-the-fly" detection with high sensitivity by combining with diversified fluorescence signals. Compared with electrochemical and optical biosensing methods, micromotor based biosensing strategies can detect biomolecules *in situ* with a short assay time. In addition, as every micromotor is a biosensor, a batch of signals can be obtained in one assay, which enhances the detection accuracy and reproducibility, simplifies the operation and reduces the detection cost. Moreover, since the motion speed of the micromotors can be used as the detection signal and directly obtained by microscopy, the use of additional detection labels can be avoided. However, the speed signal is insensitive and can only be used for semi-quantitative analysis due to the separation of sensing and power layers and the weak change of the motion speed resulting from the mass loading of biomolecules. To overcome this problem and enhance the detec-

State Key Laboratory of Analytical Chemistry for Life Science, School of Chemistry and Chemical Engineering, Nanjing University, Nanjing 210023, P. R. China. E-mail: wujie@nju.edu.cn

†Electronic supplementary information (ESI) available: DNA sequences, apparatus, Videos S1–S4 and Fig. S1–S7. See DOI: 10.1039/c7nr01168g

tion sensitivity, a double-signal based joint readout has been developed for motor-based immunosensing of cancer biomarkers at the ng mL^{-1} level.[37]

Another way to improve the sensitivity of the speed signal is to construct the sensing and power units on the same layer, in which the recognition of the target directly affects the power unit of the micromotor. For example, a "signal on" DNA micromotor sensor has been reported, in which the power part of the micromotor is formed by the target-induced DNA hybridization.[38] Our previous work also proposed a motor-based microprobe for motion detection of DNA by the DNA displacement hybridization.[39] The motor-based microprobe was fabricated by assembling a catalase layer on the inner surface of the micromotor *via* double strand DNA. The presence of target DNA separated the double strand DNA through replacement hybridization, resulting in the release of enzyme from the microtube and a decrease of the motion speed. Although the sensitivity of the speed signal has been improved by joint construction of the sensing and power units, the improvement is limited because each target relates to only one power molecule.

Here, by constructing multiple catalase layers on the inner surface of a poly(3,4-ethylenedioxythiophene and sodium 4-styrenesulfonate)/Au microtube (PEDOT-PSS/Au), an efficient enzyme-powered micromotor device was proposed for simple and sensitive detection of DNA (Scheme 1). DNA assembly could be achieved by hybridization chain reaction,[40–43] DNA super-sandwich assembly,[44–46] and catalyzed hairpin assembly,[47] and has been widely used to amplify the detection signals for ultrasensitive biosensing. In this work, cyclic alternate hybridization assembly was firstly employed for constructing a controllable multi-layer DNA architecture on the inner layer of microtubes, which served as both the power unit of the micromotor and DNA-based sensing unit (Scheme 1A). As the power unit contained multiple catalase layers, the proposed micromotor device showed excellent motion performance in H_2O_2 at low concentrations. In addition, compared with the previous work,[38,39] the introduction of cyclic alternate hybridization greatly enhanced the detection sensitivity of the micromotor device. Thus the micromotor devices showed advantages of good reproducibility, stability, and detection sensitivity, and could be an excellent candidate for rapid and simple detection of biomolecules.

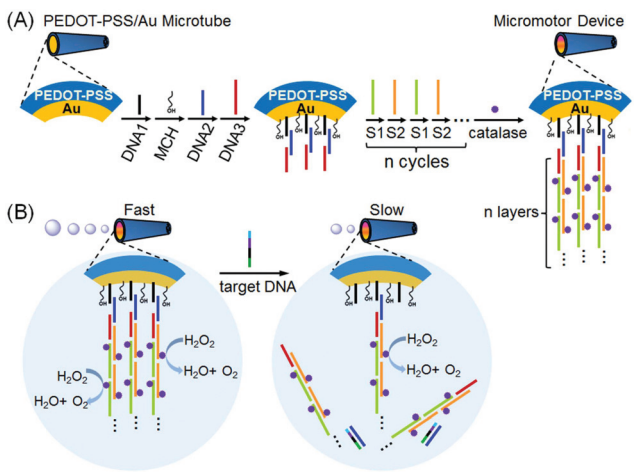

Scheme 1 Schematic representation of (A) fabrication of the micromotor device *via* cyclic alternate hybridization assembly and (B) detection of target DNA based on the motion speed readout.

Experimental

Materials and reagents

Catalases from bovine liver, poly-sodium 4-styrenesulfonate (PSS), 3,4-ethylenedioxythiophene (EDOT), *N*-hydroxycinimide (NHS), 1-ethyl-3-(3-dimethylaminopropyl) carbodiimide hydrochloride (EDC), tris (2-carboxyethyl) phosphine hydrochloride (TCEP), 6-mercapto-1-hexanol (MCH) and brilliant blue R were obtained from Sigma-Aldrich Chemical Co. (St Louis, MO, USA). Gold plating solution was gifted by Professor Wang Wei at Harbin Institute of Technology (Shenzhen). Sodium cholate hydrate (NaCh) was purchased from Alfa Aesar China Ltd. Sodium dodecyl sulfate (SDS) was purchased from Shanghai Reagent Co. (Shanghai, China). Other reagents were of analytical grade and used as received. Ultrapure water obtained from a Millipore water purification system (≥18 MΩ, Milli-Q, Millipore) was used in all experiments. PBS (10 mM, pH 7.2) containing 100 mM NaCl and 5 mM $MgCl_2$ was used for DNA hybridization. Blocking buffer was 10 mM PBS (pH 7.2) containing 0.5 mM MCH. PBS (10 mM, pH 5.5) was used as coupling buffer for the modification of catalase on DNA, and PBS (10 mM, pH 7.2) was used as washing buffer. DNA sequences are shown in the ESI.†

Preparation of the PEDOT-PSS/Au microtube

The PEDOT-PSS/Au microtube was prepared following the template directed electrodeposition protocol.[48] Briefly, a 75 nm-thick gold film was firstly sputtered on the smooth side of the polycarbonate membrane (with 5 μm-diameter micropores, Catalog No 7060-2513, Whatman USA). Then, the membrane was assembled in an electrochemical plating cell using an aluminum foil and served as a working electrode. On the wall of the micropores, PEDOT-PSS was firstly electropolymerized at +0.80 V (*vs.* SCE) to a charge of 0.30 C in a plating solution containing 15 mM EDOT, 7.5 mM KNO_3, 100 mM SDS, and 7 mg mL^{-1} PSS. Subsequently, the inner Au layer was deposited at −1.1 V (*vs.* Ag/AgCl) for 1800 s in the gold plating solution. The sputtered gold film was then completely removed from the template membrane by hand polishing with alumina slurry. After dissolving the membrane in methylene chloride for 30 min, the PEDOT-PSS/Au microtubes were obtained with a sequential wash with methylene chloride, ethanol and ultrapure water and stored in ultrapure water at room temperature before use.

Preparation of the micromotor device through cyclic alternate hybridization assembly

Firstly, SH-DNA1 (5 μM) was treated in 0.75 mM TCEP for 2 h, and incubated with PEDOT-PSS/Au microtubes overnight for

immobilization on the inner Au layer *via* Au–S binding (Scheme 1). After washing with washing buffer, the microtubes were dispersed in blocking buffer for 1 h to block possible nonspecific sites of the inner Au layer and optimize the orientation of the DNA1. Then the microtubes were washed and sequentially incubated in a solution of 5 μM DNA2 and DNA3 to construct the sensing unit. Afterwards, the microtubes were alternately hybridized with 20 μM S1 and S2 for 30 min, and the process was cycled 5 times to form a DNA assembly layer. Next, the microtubes were incubated in coupling buffer containing 0.4 M EDC and 0.1 M NHS for 1 h to activate the carboxyl group modified on S1 and S2, followed by a 7 h incubation in 5 mg mL^{-1} catalase. After washing with washing buffer, the micromotor devices were finally obtained and stored in PBS (pH 7.0) at 4 °C prior to use.

Stability characterization of catalase immobilized on the micromotor

After 20 μL of micromotor devices or 0.01 mg mL^{-1} catalase was dispersed in 40 μL PBS containing 1.25% NaCh and 3% H_2O_2 for a given time, 5 μL of the solution was diluted 60 times with PBS to determine the decomposition percentage of H_2O_2 with UV absorption at 240 nm.

Detection of target DNA

The micromotor devices were firstly incubated with target DNA of different concentrations at 37 °C for 30 min to ensure the sufficient displacement hybridization and release of the DNA assembly along with the multi-catalase. Then, 2 μL of the micromotor devices were mixed with 4 μL of fuel solution containing 3% H_2O_2 and 1.25% NaCh and subsequently cast on a glass slide for immediate observation by using an inverted optical microscope. The motion speed of the micromotor device was calculated by dividing the object's center-to-center displacement from frame to frame by the time interval.

Results and discussion

Characterization of the PEDOT-PSS/Au microtube

The SEM morphology of the PEDOT-PSS/Au microtube showed a defined cone tubular shape with a uniform, compact and smooth outer surface and a rough inner surface (Fig. 1A and B). The microtubes had a length of ~13.5 μm and an inner opening of ~3.0 μm, which was big enough for construction of the DNA assembly with multi-catalase in the inner surface. The composition of the microtube was characterized by energy dispersive X-ray (EDX) analysis, which showed a uniform distribution of element S (Fig. 1C), C (Fig. 1D) and Au (Fig. 1E) within the microtube, indicating the successful preparation of PEDOT-PSS/Au microtubes.

For successful fabrication of the micromotor device by cyclic alternate DNA hybridization assembly, the nonspecific adsorption of DNA strands on the outer polymeric surface of the microtubes should be eliminated. Here, the negatively charged PSS was employed to dope with positively charged

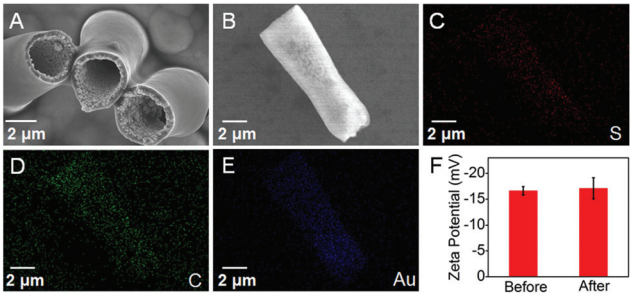

Fig. 1 SEM images of PEDOT-PSS/Au microtubes from (A) top and (B) side view. EDX mapping analysis of (C) sulfur, (D) carbon and (E) Au of the PEDOT-PSS/Au microtube. (F) Zeta potential analysis of the PEDOT-PSS microtube before and after an overnight incubation with 5 μM DNA strands.

PEDOT and co-electropolymerized to form the polymeric layer. In this work, PEDOT-PSS microtubes without the Au inner layer were synthesized and dispersed in PBS (10 mM, pH 7.2) for zeta potential analysis (Fig. 1F). The microtubes fabricated with the PEDOT-PSS polymeric layer were negatively charged, and few potential changes were observed after overnight incubation with 5 μM DNA strands in PBS (10 mM, pH 7.2) followed by centrifugation washings with washing buffer to remove excess DNA, indicating that no DNA nonspecifically adsorbed on the negatively charged PEDOT-PSS layer.

Feasibility of fabrication and detection of the micromotor device

The micromotor device was fabricated by using cyclic alternate hybridization assembly to construct both sensing and power units on the inner Au surface of the PEDOT-PSS/Au microtube. The recognition of the target DNA broke the sensing unit and caused the separation of the power unit from the micromotor, resulting in a decrease of motion speed. The detailed DNA assembly and target recognition process are shown in Fig. S1 in the ESI.† Here, DNA2 was designed as the sensing unit, which contained 12 complementary bases to DNA1 and DNA3, respectively. S1 and S2 that could alternately hybridize with each other to form a multi-layer DNA architecture were used to construct the power unit. DNA1 was used to capture the sensing unit DNA2 on the surface of the Au layer and DNA3 that contained another 21 bases complementary to S1 was designed to construct the multi-layer DNA architecture on DNA2. As the target DNA was full complementary (36 complementary bases) to DNA2, it could hybridize with DNA2 to form the target/DNA2 double strand, which released the multi-layer DNA architecture of DNA3/S1/S2···S1/S2.

Polyacrylamide gel electrophoresis (PAGE) analysis was performed to verify the feasibility of these DNA hybridization reactions (Fig. 2). The mixture of S1 and S2 showed a typical striped production (Fig. S2†), suggesting the alternate hybridization of S1 and S2 and the formation of multi-layer DNA assembly of S1/S2···S1/S2. In contrast, compared to the single strand DNA (Fig. 2B, lanes a–d), only one clear band with

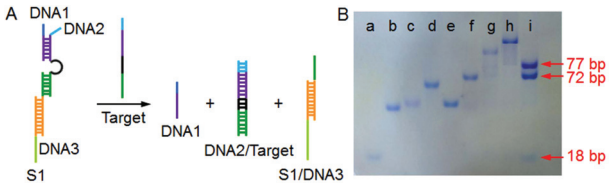

Fig. 2 (A) Schematic representation of target DNA displacement hybridization with DNA2 and the release of S1/DNA3. (B) Gel electrophoresis image of (a) DNA1, (b) DNA2, (c) DNA3, (d) S1, (e) target DNA, the mixture of (f) DNA1 and DNA2, (g) DNA1, DNA2 and DNA3, and (h) DNA1, DNA2, DNA3 and S1, and (i) (h) + target DNA.

slower migration was observed for the mixture of DNA1 and DNA2 (lane f), DNA1, DNA2 and DNA3 (lane g), and DNA1, DNA2, DNA3 and S1 (lane h), respectively. In addition, the band turned slower in order from lanes f to h. These bands should correspond to the DNA1/DNA2 double strand, DNA1/DNA2/DNA3 and DNA1/DNA2/DNA3/S1 assemblies, respectively, suggesting the successful hybridization among DNA1, DNA2, DNA3 and S1. However, the mixture of target DNA with DNA1/DNA2/DNA3/S1 assembly showed three bands corresponding to 18, 72 and 77 bases (lane i), which were attributed to the presence of DNA 1, DNA2/target and S1/DNA3, respectively. This result indicated that the target DNA could displacement hybridize with DNA2 and release the DNA3-based assembly. Thus, the feasibility of the fabrication and detection ability of the micromotor device by cyclic alternate DNA hybridization assembly was confirmed.

Fabrication of the micromotor device

In order to achieve highly efficient micromotor devices, the motion performance of the micromotors with different preparation processes was investigated. Here, three kinds of micromotor devices were fabricated (Fig. 3A). For the first kind of micromotor device, the power unit was constructed without multi-layer DNA assembly (Fig. 3A-a), in which each sensing unit could only couple with one DNA assembly layer of S1/S2′, thus a small amount of catalase would be modified on the inner surface of micromotors, leading to a slow motion speed of 240 ± 14 μm s^{-1} (Fig. 3B-a). Furthermore, a small decrease of the speed (~27 μm s^{-1}) was observed in the presence of 500 nM target DNA (Fig. 3B-a), suggesting that this kind of micromotor device was insensitive to target DNA.[38,39]

The second kind of micromotor device was fabricated by controllable DNA assembly relying on the cyclic alternate hybridization of S1 and S2 (Fig. 3A-b). For this kind of micromotor device, each sensing unit coupled with multiple DNA layers along with a high amount of catalase, hence it was faster and more sensitive than the first kind of micromotor. However, the motion speed of this kind of micromotor greatly depended on the cyclic number of the alternate hybridization between S1 and S2. With the increasing cyclic number of the alternate hybridization, the motion speed of the micromotors increased sharply and reached the maximum speed of 420 ± 18 μm s^{-1} at the cyclic number of 5 (Fig. 3B-b). In addition,

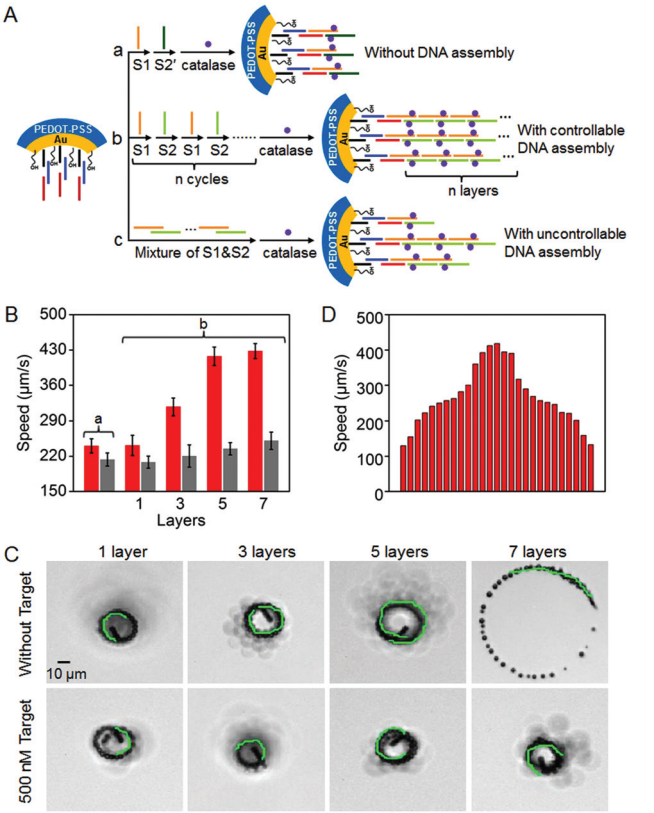

Fig. 3 (A) Schematic representation of micromotor device fabrication (a) without and with (b) controllable and (c) uncontrollable DNA assembly. (B) Speeds of micromotor devices fabricated (a) without and (b) with DNA assembly at different cycles in the absence (red column) and presence (gray column) of 500 nM target DNA. Error bars represented the standard deviations from 10 micromotor devices. (C) Tracking trajectories of micromotor devices with different DNA assembly layers in the absence and presence of target DNA during a period of 0.2 s. (D) Motion speeds of 27 micromotor devices constructed by uncontrollable DNA assembly.

the speed decrease of the micromotor device in the presence of 500 nM target DNA was sharply increased from 33 μm s^{-1} at 1 cycle to 183 μm s^{-1} at 5 cycles. These results indicated that the micromotor devices prepared with 5 cycles showed the best motion and detection performance. Fig. 3C shows the tracking trajectories of micromotor devices prepared with different cycles of alternate hybridization of S1 and S2 in the absence and presence of target DNA during a period of 0.2 s (also shown in the ESI, Video S1†). Similar to the previous work,[49] the trajectories of the present micromotor devices are circular due to both the constant force/torque produced by the catalytic layer[50] and the high Reynolds number of the system.[51]

The third kind of micromotor device was fabricated by an uncontrollable DNA assembly, in which S1 and S2 were mixed firstly to form long DNA assemblies and then these DNA chains were captured with DNA3 to serve as the power unit (Fig. 3A-c). Because the mixture of S1 and S2 could produce DNA assemblies in different lengths, for example assemblies

of S1/S2, S1/S2/S1, S1/S2/S1/S2, and S1/S2···S1/S2, the DNA assembly as well as the amount of catalase on each sensing unit were nonuniform, resulting in a big difference of the motion speeds of micromotor devices fabricated in the same batch (Fig. 3D and Video S2†). The poor uniformity and reproducibility of the micromotor devices fabricated by uncontrollable DNA assembly made them unsuitable for biosensing applications.

In view of the above results, the micromotor devices fabricated with the controllable DNA assembly and 5 cyclic alternate hybridization of S1 and S2 were used for all the experiments. Here, catalase was conjugated to the DNA assemblies of S1/S2···S1/S2 *via* EDC and NHS assisted reaction to construct the power unit of the micromotor device. The conjugation of catalase to DNA was verified by PAGE experiment (Fig. S3†). One thing to note, in this work, the Au layer was introduced only to facilitate the modification of DNA1 and further the construction of a DNA architecture as well as catalase layers on the inner surface of the microtubes, thus it could be replaced with other materials which possessed active binding sites for DNA, for example polymers with amino or carboxyl groups.

Optimization of preparation and detection conditions

As shown in Fig. 4A, the speed of the micromotor increased with the increasing DNA1 concentration and tended to a steady state when the concentration of DNA1 was beyond 5 μM. Thus, 5 μM DNA1 was selected for the preparation of micromotor devices. It was worth noting that the efficiency of Au–S bonding was affected by the ionic concentration of the reaction solution. Here, PBS (10 mM, pH 7.2) containing 1 M KH_2PO_4 was used for the assembly of DNA1 on the inner Au surface of the PEDOT-PSS/Au microtube. According to the DNA1 concentration, 5 μM DNA2 and DNA3 were used in this work.

S1 and S2 were orderly assembled on the inner surface of the microtube and then conjugated with catalase to construct the power unit of the micromotor. As the power unit decided the motion and detection performances of the micromotor, the concentrations of S1, S2 and catalase were also optimized. In this study, S1 and S2 were at the same concentration. With the increasing concentrations of S1, S2, and catalase, the motion speed of the micromotor device increased sharply and reached the maximum value at 20 μM S1 and S2 and 5 mg mL^{-1} catalase (Fig. 4B and C). Hence, the concentrations of 20 μM and 5 mg mL^{-1} were selected for S1 and S2, and catalase, respectively.

The dependence of the motion speed of the micromotor device on the temperature of detection solution was investigated. Here, the temperature of detection solution was controlled through an intelligent temperature control device equipped on the microscope. The fastest speed was observed at 37 °C due to the highest catalytic ability of catalase (Fig. 4D). Thus, all the motion speeds were observed at 37 °C.

Besides, the motion performance of micromotor devices in H_2O_2 fuel at different concentrations was observed (Fig. 5, Video S3†). Similar to the reported enzyme-powered micromotors,[39] the velocity of the micromotor devices increased with the increase of H_2O_2 concentration and trended the maximum value at 2%. Considering the stability or activity of the immobilized catalase, a low concentration of H_2O_2 was appropriate, and the motion performance of micromotors in $H_2O_2 \leq$ 2% was extremely important. The proposed micromotor devices showed a motion speed of ~420 μm s^{-1} in 2% H_2O_2, which was much higher than other enzyme-powered micromotors.[39,49,52]

In the presence of 2% H_2O_2, the micromotor devices could maintain a constant motion speed over 2 min (Fig. S4†), indicating the acceptable stability for the assay process of several seconds upon mixing with H_2O_2. Moreover, the micromotor devices also showed a good motion performance in 0.25% H_2O_2 with a speed of ~51 μm s^{-1}. The nice motion ability of the micromotor devices was attributed to the programmed multi-layer DNA assembly on the inner Au surface, which

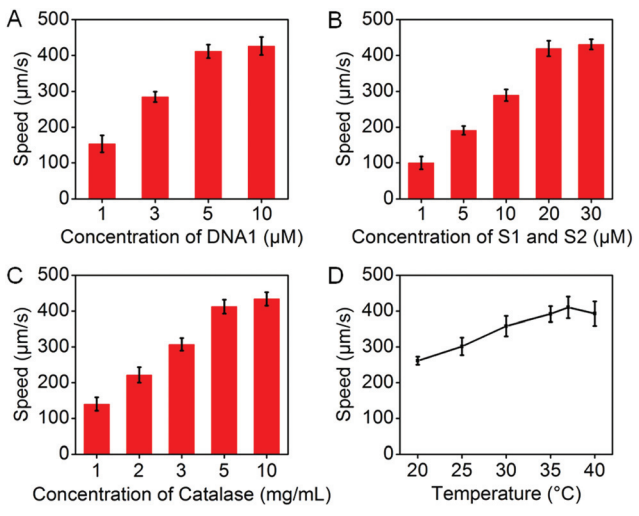

Fig. 4 Dependence of the motion speed of micromotor devices on concentrations of (A) DNA1, (B) S1 and S2, and (C) catalase, and (D) temperature of detection solution. Error bars represented the standard deviations of the speed from 10 micromotor devices.

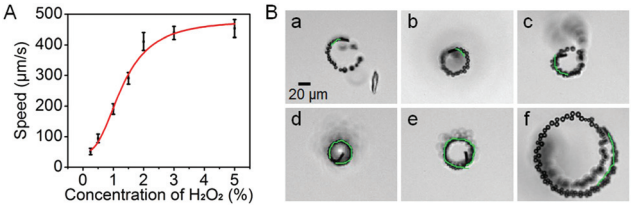

Fig. 5 (A) Dependence of the motion speed of the micromotor device on the H_2O_2 concentration. (B) Time-lapse images of the motion of micromotor devices in the presence of H_2O_2 at concentrations of (a) 0.25%, (b) 0.5%, (c) 1%, (d) 1.5%, (e) 2% and (f) 3% during a period of 0.2 s. Error bars represented the standard deviations of the speed from 10 micromotor devices.

enabled the labeling of multiple catalase and hence the construction of the efficient power unit of the micromotor.

To further demonstrate the stability of the immobilized catalase, its activity for decomposing H_2O_2 in the presence of 2% H_2O_2 was examined. The decomposition percentage of 2% H_2O_2 linearly increased in the initial 3 min and then gradually trended a flat (Fig. S5†), indicating the decrease of enzymatic activity after 3 min. In contrast, the decomposition percentage for native catalase remained almost unchanged after 1 min. Thus, the immobilized catalase showed better stability and could maintain its activity in 2% H_2O_2 for 3 min. The former was also verified by exposing the micromotor or native catalase to 2% H_2O_2 every 10 min (Fig. S6†) or applying the native or conjugated catalase exposed to 2% H_2O_2 to decompose 11 mM H_2O_2 (Fig. S7†). These results were consistent with those in previous reports.[52–54]

Assay performance

Under the optimized conditions, the velocity of the micromotor devices decreased with the increasing concentration of target DNA (Fig. 6A). The motion performance of the micromotor devices in response to target DNA at different concentrations is shown in Fig. 6B and Video S4.† The motion speed showed a low power exponential function relationship with the target DNA concentration from 10 to 1000 nM with the regression equation of $S = 401.18 - 4.28C^{0.59}$ (the correlation coefficient was 0.9976). Although the exponential value of the motion readout (0.59) was lower than 1, it was much higher than 0.18 obtained in the previous work,[39] suggesting that the micromotor devices fabricated with the cyclic alternate DNA hybridization assembly greatly improved the detection sensitivity. In addition, due to the high motion performance of the micromotor devices, the detection limit of the target DNA was also 50 times lower than those in previous work.[38,39] These results indicated that the cyclic alternate hybridization assembly was an efficient technique for the fabrication of micromotor devices with excellent motion and biosensing abilities. Although the detection limit was not as satisfactory as those of other detection methods such as electrochemical and fluorescence detection, it could be greatly enhanced with a more precise DNA assembly. Additionally, as the sensing unit was constructed by the DNA assembly, the micromotor devices could be extended to detect a variety of other biomolecules, such as proteins.

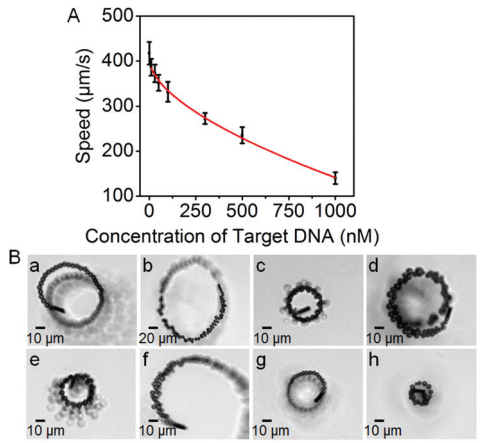

Fig. 6 (A) Relationship between motion speed and DNA concentration from 10 nM to 1 μM. (B) Time-lapse images of micromotor devices in response to 0 (a), 10 (b), 30 (c), 50 (d), 100 (e), 300 (f), 500 (g) and 1000 (h) nM target DNA during a period of 0.2 s. Error bars represented the standard deviations of speed from 10 micromotor devices.

Stability, reproducibility, selectivity and real sample analysis of the micromotor devices

Stability was tested by examining the motion speeds of 10 micromotor devices against the storage time (Fig. 7A). The speed of the micromotor devices slightly changed during 3 weeks. Moreover, the speed in response to 500 nM target DNA was also constant, suggesting the good stability of the micromotor devices.

To test their reproducibility, the micromotor devices prepared from the same batch and different three batches were used to detect 500 nM target DNA. The micromotor devices showed reproducible motion speeds of 418 ± 25 μm s^{-1} and 236 ± 18 μm s^{-1} with relative standard deviations (RSD) of 5.99% and 7.63% in response to 0 and 500 nM target DNA, respectively. These results indicated that the micromotor devices possessed good reproducibility of both preparation and detection.

The specificity of the micromotor device for DNA detection was verified by measuring target DNA, single-base mismatch DNA, three-bases mismatch DNA, and non-complementary DNA (Fig. 7B). A big decrease of the motion speed was observed when micromotor devices were treated with target DNA and single-base mismatch DNA, while a slight change of the motion speed was observed when micromotor devices were incubated with three-bases mismatch DNA and non-complementary DNA, suggesting that the proposed micromotor devices could selectively distinguish target DNA from multi-base mismatched DNA.

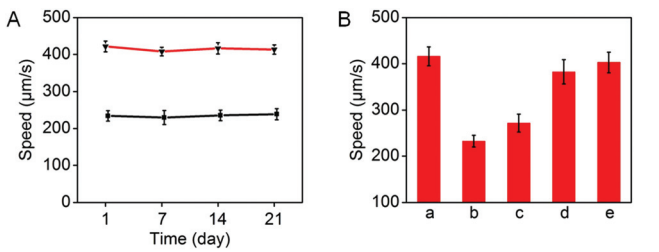

Fig. 7 (A) Dependence of the motion speed of micromotor devices in the absence (up) and presence (down) of 500 nM target DNA on the storage time at 4 °C. (B) Motion speed of micromotor devices in response to (a) 0 and (b) 500 nM target DNA, (c) 5 μM single-base mismatch DNA, (d) 5 μM three-base mismatch DNA and (e) 5 μM non-complementary DNA. Error bars represented the standard deviations of the speed from 10 micromotor devices.

To assess the application of the micromotor devices in complex biological systems, the analysis of target DNA spiked in clinical serum samples was performed. The micromotor devices showed a good motion performance in the serum sample. The concentrations of target DNA determined according to the regression equation obtained above were in good agreement with the actual values. The relative recovery was 90.8%, indicating good detection accuracy of the micromotor devices.

Conclusions

This work proposes an efficient enzyme-powered micromotor device through cyclic alternate hybridization DNA assembly. Due to the programmed DNA assembly, a controllable multilayer DNA architecture is constructed for further conjugation with catalase to form the efficient power unit of the micromotor. Benefitting from the mutli-catalase layers, the proposed micromotor device shows excellent motion performance in H_2O_2 at low concentrations. In addition, target DNA recognition to the micromotor device can release the multiple power molecules, hence the detection sensitivity of the micromotor device is greatly enhanced. Moreover, by designing the DNA architecture with specific DNA strands or other affinity linkers, the micromotor devices can be conveniently extended to detect a variety of biomolecules. The micromotor devices show good selectivity and reproducibility, excellent stability and good assay performance in biological media, indicating an excellent detection tool for biosensing application.

Acknowledgements

We gratefully acknowledge the National Natural Science Foundation of China (21575063 and 21361162002), the Program for New Century Excellent Talents in University of Ministry of Education of China (NCET-13-0283) and the Independent Research Foundation from State Key Laboratory of Analytical Chemistry for Life Science (5431ZZXM1610).

Notes and references

1 B. H. Dai, J. Z. Wang, Z. Xiong, X. J. Zhan, W. Dai, C. C. Li, S. P. Feng and J. Y. Tang, *Nat. Nanotechnol.*, 2016, **11**, 1087.
2 G. A. Ozin, I. Manners, S. Fournier-Bidoz and A. Arsenault, *Adv. Mater.*, 2005, **17**, 3011.
3 H. Wang and M. Pumera, *Chem. Rev.*, 2015, **115**, 8704.
4 K. Kim, J. H. Guo, X. B. Xu and D. L. Fan, *Small*, 2015, **11**, 4037.
5 M. Guix, C. C. Mayorga-Martinez and A. Merkoçi, *Chem. Rev.*, 2014, **114**, 6285.
6 S. Sánchez, L. Soler and J. Katuri, *Angew. Chem., Int. Ed.*, 2015, **54**, 1414.
7 W. F. Paxton, K. C. Kistler, C. C. Olmeda, A. Sen, S. K. S. Angelo, Y. Y. Cao, T. E. Mallouk, P. E. Lammert and V. H. Crespi, *J. Am. Chem. Soc.*, 2004, **126**, 13424.
8 S. Fournier-Bidoz, A. C. Arsenault, I. Manners and G. A. Ozin, *Chem. Commun.*, 2005, 441.
9 S. J. Wang and N. Wu, *Langmuir*, 2014, **30**, 3477.
10 Y. Wang, R. M. Hernandez, D. J. Bartlett, J. M. Bingham, T. R. Kline, A. Sen and T. E. Mallouk, *Langmuir*, 2006, **22**, 10451.
11 A. A. Solovev, Y. F. Mei, E. B. Ureña, G. H. Huang and O. G. Schmidt, *Small*, 2009, **5**, 1688.
12 W. Wang, W. T. Duan, S. Ahmed, T. E. Mallouk and A. Sen, *Nano Today*, 2013, **8**, 531.
13 M. J. Xuan and Q. He, *ChemPhysChem*, 2014, **15**, 2255.
14 Z. G. Wu, X. K. Lin, X. Zou, J. M. Sun and Q. He, *ACS Appl. Mater. Interfaces*, 2015, **7**, 250.
15 W. Gao and J. Wang, *Nanoscale*, 2014, **6**, 10486.
16 V. Garcia-Gradilla, S. Sattayasamitsathit, F. Soto, F. Kuralay, C. Yardımcı, D. Wiitala, M. Galarnyk and J. Wang, *Small*, 2014, **10**, 4154.
17 D. L. Fan, Z. Z. Yin, R. Cheong, F. Q. Zhu, R. C. Cammarata1, C. L. Chien and A. Levchenko, *Nat. Nanotechnol.*, 2010, **5**, 545.
18 S. Balasubramanian, D. Kagan, L. F. Zhang and J. Wang, *Angew. Chem., Int. Ed.*, 2011, **50**, 4161.
19 S. Campuzano, J. Orozco, D. Kagan, M. Guix, W. Gao, S. Sattayasamitsathit, J. C. Claussen, A. Merkoci and J. Wang, *Nano Lett.*, 2012, **12**, 396.
20 F. Kuralay, S. Sattayasamitsathit, W. Gao, A. Uygun, A. Katzenberg and J. Wang, *J. Am. Chem. Soc.*, 2012, **134**, 15217.
21 W. Gao, X. Feng, A. Pei, Y. Gu, J. X. Li and J. Wang, *Nanoscale*, 2013, **5**, 4696.
22 S. K. Srivastava, M. Guix and O. G. Schmidt, *Nano Lett.*, 2016, **16**, 817.
23 L. Soler and S. Sanchez, *Nanoscale*, 2014, **6**, 7175.
24 M. Guix, J. Orozco, M. Garcia, W. Gao, S. Sattayasamitsathit, A. Merkoci, A. Escarpa and J. Wang, *ACS Nano*, 2012, **6**, 4445.
25 J. Orozco, G. Cheng, D. Vilela, S. Sattayasamitsathit, R. Vazquez-Duhalt, G. Valdes-Ramirez, O. S. Pak, A. Escarpa, C. Kan and J. Wang, *Angew. Chem., Int. Ed.*, 2013, **52**, 13276.
26 L. Soler, V. Magdanz, V. M. Fomin, S. Sanchez and O. G. Schmidt, *ACS Nano*, 2013, **7**, 9611.
27 V. V. Singh, F. Soto, K. Kaufmann and J. Wang, *Angew. Chem., Int. Ed.*, 2015, **54**, 6896.
28 D. Kagan, P. Calvo-Marzal, S. Balasubramanian, S. Sattayasamitsathit, K. M. Manesh, G. U. Flechsig and J. Wang, *J. Am. Chem. Soc.*, 2009, **131**, 12082.
29 J. Wu, S. Balasubramanian, D. Kagan, K. M. Manesh, S. Campuzano and J. Wang, *Nat. Commun.*, 2010, **1**, 36.
30 J. Wang and W. Gao, *ACS Nano*, 2012, **6**, 5745.
31 W. Gao, S. Sattayasamitsathit, J. Orozco and J. Wang, *J. Am. Chem. Soc.*, 2011, **133**, 11862.

32 Y. F. Mei, G. S. Huang, A. A. Solovev, E. B. Ureña, I. Mönch, F. Ding, T. Reindl, R. K. Y. Fu, P. K. Chu and O. G. Schmidt, *Adv. Mater.*, 2008, **20**, 4085.
33 S. Campuzano, D. Kagan, J. Orozco and J. Wang, *Analyst*, 2011, **136**, 4621.
34 E. Morales-Narváez, M. Guix, M. Medina-Sánchez, C. C. Mayorga-Martinez and A. Merkoçi, *Small*, 2014, **10**, 2542.
35 D. Kagan, S. Campuzano, S. Balasubramanian, F. Kuralay, G. Flechsig and J. Wang, *Nano Lett.*, 2011, **11**, 2083.
36 B. E. Ávila, M. A. Lopez-Ramirez, D. F. Báez, A. Jodra, V. V. Singh, K. Kaufmann and J. Wang, *ACS Sens.*, 2016, **1**, 217.
37 X. P. Yu, Y. N. Li, J. Wu and H. X. Ju, *Anal. Chem.*, 2014, **86**, 4501.
38 K. V. Nguyen and S. D. Minteer, *Chem. Commun.*, 2015, **51**, 4782.
39 Y. Z. Xie, S. Z. Fu, J. Wu, J. P. Lei and H. X. Ju, *Biosens. Bioelectron.*, 2017, **87**, 31.
40 J. J. Guo, J. C. Wang, J. Q. Zhao, Z. L. Guo and Y. Z. Zhang, *ACS Appl. Mater. Interfaces*, 2016, **8**, 6898.
41 B. Zhang, B. Q. Liu, D. P. Tang, R. Niessner, G. N. Chen and D. Knopp, *Anal. Chem.*, 2012, **84**, 5392.
42 Z. Wu, G. Q. Liu, X. L. Yang and J. H. Jiang, *J. Am. Chem. Soc.*, 2015, **137**, 6829.
43 L. Tong, J. Wu, J. Li, H. X. Ju and F. Yan, *Analyst*, 2013, **138**, 4870.
44 X. Chen, Y. H. Lin, J. Li, L. S. Lin, G. N. Chen and H. H. Yang, *Chem. Commun.*, 2011, **47**, 12116.
45 J. Wang, A. Q. Shi, X. Fang, X. W. Han and Y. Z. Zhang, *Anal. Biochem.*, 2015, **469**, 71.
46 F. Xia, R. J. White, X. L. Zuo, A. Patterson, Y. Xiao, D. Kang, X. Gong, K. W. Plaxco and A. J. Heeger, *J. Am. Chem. Soc.*, 2010, **132**, 14346.
47 Y. H. Guo, J. Wu and H. X. Ju, *Chem. Sci.*, 2015, **6**, 4318.
48 W. Gao, S. Sattayasamitsathit, A. Uygun, A. Pei, A. Ponedal and J. Wang, *Nanoscale*, 2012, **4**, 2447.
49 J. Orozco, V. García-Gradilla, M. D'Agostino, W. Gao, A. Cortés and J. Wang, *ACS Nano*, 2013, **7**, 818.
50 Z. Zhang, J. H. Li, L. W. Fu, D. Y. Liu and L. X. Chen, *J. Mater. Chem. A*, 2015, **3**, 7437.
51 G. J. Zhao, N. T. Nguyen and M. Pumera, *Nanoscale*, 2013, **5**, 7277.
52 S. Sanchez, A. A. Solovev, Y. F. Mei and O. G. Schmidt, *J. Am. Chem. Soc.*, 2010, **132**, 13144.
53 J. Simmchen, A. Baeza, D. Ruiz-Molina and M. Vallet-Regi, *Nanoscale*, 2014, **6**, 8907.
54 M. Yan, J. J. Du, Z. Gu, M. Liang, Y. F. Hu, W. J. Zhang, S. Priceman, L. Wu, Z. H. Zhou, Z. Liu, T. Segura, Y. Tang and Y. F. Lu, *Nat. Nanotechnol.*, 2010, **5**, 48.